

Anomalous Hopf Bifurcations in Symmetrically-coupled Period-doubling Systems

Woochang Lim* and Sang-Yoon Kim†

Department of Physics, Kangwon National University, Chunchon 200-701

We consider two symmetrically-coupled logistic maps, and investigate the effect of symmetry on Hopf bifurcations, giving rise to the birth of the daughter orbits encircling the symmetric anti-phase mother orbit (with a time shift of half a period). When the rotation numbers ν of daughter orbits are rational (*i.e.*, $\nu = r/s$; r and s : coprimes), anomalous Hopf bifurcations are found to occur due to the symmetry of the coupled system. For even r , a symmetric periodic attractor is born through a standard Hopf bifurcation while for odd r , a conjugate pair of asymmetric periodic attractors appears via a nonstandard double Hopf bifurcation. These symmetry-conserving and -breaking Hopf bifurcations are explained by using the concept of a half-cycle map of a symmetrically-coupled map. These anomalous Hopf bifurcations might be observed in real experiments of symmetrically-coupled period-doubling systems.

PACS numbers: 05.45.Ac

Keywords: Anomalous Hopf bifurcations, Symmetrically-coupled period-doubling systems

DOI: 10.3938/jkps.56.711

I. INTRODUCTION

Two coupled oscillators with competing frequencies exhibit a typical transition from quasiperiodicity to chaos as the coupling strength passes a threshold value. As a representative model for the quasiperiodic transition to chaos, the circle map has been intensively studied [1,2]. We note that such a quasiperiodic transition occurs in two symmetrically coupled period-doubling systems. The dynamics of two coupled logistic maps [3–7] and two coupled Rössler oscillators [8], which individually display a period-doubling transition to chaos, has been investigated in details. Thus, a quasiperiodic transition to chaos (accompanied with mode lockings) has been found, as in the case of the circle map. This interesting phenomenon has been observed experimentally in two resistively-coupled p-n junction resonators [9]. The coupled resonators show a quasiperiodic transition through replacement of period-doubling bifurcations of the single resonator with Hopf bifurcations. A similar quasiperiodic transition to chaos was also observed in an experiment involving two inductively coupled electronic frequency generators [10].

Emergence of Hopf bifurcations was shown to be a generic feature of symmetrically-coupled period-doubling systems [11,12]. However, so far the type of daughter orbit that appears via these Hopf bifurcations remains unclear. To make this point clear, in Sec. II, we investi-

gate the effect of symmetry on Hopf bifurcations of symmetric anti-phase mother orbits in two symmetrically-coupled logistic maps. When the rotation numbers ν of daughter orbits (which are just the average numbers of rotations around a mother orbit point per period of the mother orbit) are rational (*i.e.*, $\nu = r/s$; r and s : coprimes), two types of Hopf bifurcations are found to occur. For even r , a symmetric periodic attractor is born through a standard Hopf bifurcation while for odd r , a conjugate pair of asymmetric periodic attractors appears via a nonstandard double Hopf bifurcation. We explain the symmetry-conserving and -breaking Hopf bifurcations by using the concept of a half-cycle map of the symmetrically-coupled map [13]. These anomalous Hopf bifurcations are expected to be observed in experiments of symmetrically-coupled period-doubling systems, such as two resistively-coupled p-n junction resonators [9] and two inductively-coupled electronic frequency generators [10]. Finally, we give a summary in Sec. III.

II. SYMMETRY-CONSERVING AND -BREAKING HOPF BIFURCATIONS IN TWO COUPLED LOGISTIC MAPS

We consider two symmetrically-coupled period-doubling maps:

$$T : \begin{cases} x_{n+1} = f(x_n) + \varepsilon(y_n - x_n), \\ y_{n+1} = f(y_n) + \varepsilon(x_n - y_n), \end{cases} \quad (1)$$

*E-mail: wclim@kangwon.ac.kr

†Corresponding author; E-mail: sykim@kangwon.ac.kr

where x_n and y_n are state variables of the first and the second elements at a discrete time n , and ε is a coupling parameter. As an element in our coupled system, we choose the one-dimensional logistic map with $f(x) = 1 - ax^2$, which is a representative period-doubling system [14]. In the single logistic map, a period-doubling transition to chaos occurs as the nonlinearity parameter a passes a threshold value $a^* (= 1.401\ 155 \dots)$. We also note that the coupled map T has an exchange symmetry S such that

$$STS(x, y) = T(x, y); S(x, y) = (y, x). \quad (2)$$

The set of all points, which are invariant under the exchange of coordinates S , form a symmetry line $y = x$. If an orbit is invariant under S , it is called a symmetric orbit; otherwise, it is called an asymmetric orbit.

For the uncoupled case of $\varepsilon = 0$, the coupled map of Eq. (1) breaks into two uncoupled logistic maps. If they both have orbits with period P , then the composite system has P different orbits distinguished by the phase shift $Q (= 0, 1, \dots, P - 1)$. The case of $Q = 0$ corresponds to the in-phase orbit on the diagonal, while other cases of $Q \neq 0$ correspond to out-of-phase orbits. If $Q = P/2$, then an anti-phase (180° out-of-phase) orbit with a time shift of half a period exists; otherwise ($Q \neq P/2$), non-antiphase orbits appear. The in-phase and the anti-phase periodic orbits are symmetric with respect to the exchange symmetry S , while other periodic orbits are asymmetric. Two asymmetric period- P orbits with phase shift Q and $P - Q$ are conjugate ones because one orbit is transformed into the other one under the exchange of coordinates S . These orbits will be called “conjugate-phase” orbits, and they have the same stability. All periodic orbits, associated with the period-doubling cascade of the logistic map, persist when coupling is introduced, at least while its value is small enough. Hereafter, we classify these periodic orbits in terms of their periods and phase shifts (P, Q) .

The stability of an orbit with period P in two coupled maps of Eq. (1) is determined from the Jacobian matrix J of T^P , which is the P -product of the Jacobian matrix DT of T along the orbit:

$$J = \prod_{n=1}^P DT(x_n, y_n) = \prod_{n=1}^P \begin{pmatrix} f'(x_n) - \varepsilon & \varepsilon \\ \varepsilon & f'(y_n) - \varepsilon \end{pmatrix}, \quad (3)$$

where $f'(x) = df(x)/dx$. The eigenvalues of J , λ_1 and λ_2 , are called the stability multipliers of the orbit. An orbit is stable only when the moduli of both multipliers are less than unity (*i.e.*, $|\lambda_i| < 1$ ($i = 1, 2$)); both of them lie inside the unit circle in the complex plane). When a multiplier passes the unit circle at $\lambda = 1$ (-1), the orbit becomes unstable via a saddle-node or pitchfork (period-doubling) bifurcation. On the other hand, as a pair of

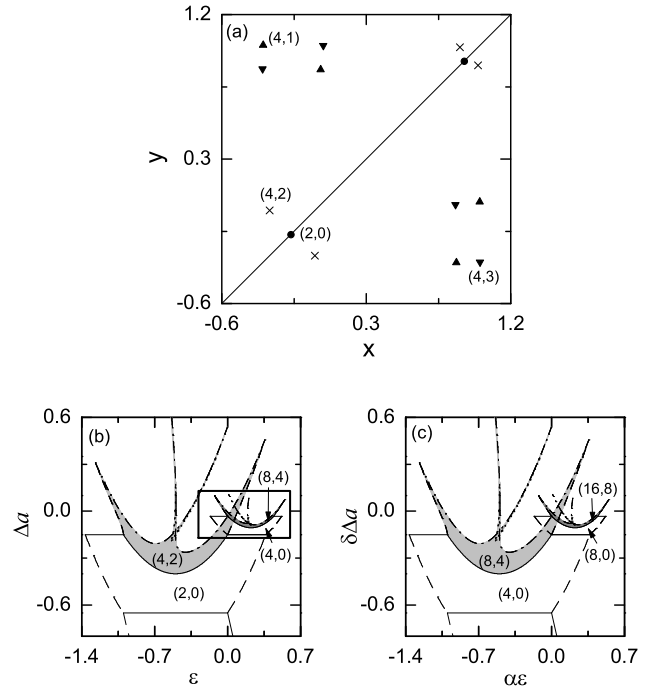


Fig. 1. (a) Periodic orbits for $a = 1.31$ and $\varepsilon = 0.01$. There are symmetric in-phase (denoted by solid circles) and anti-phase (denoted by crosses) orbits and asymmetric conjugate-phase orbits (represented by up- and down-triangles). (b) Stability diagram in the $\varepsilon - \Delta a$ plane; $\Delta a = a - a^*$ ($a^* = 1.401\ 155\ 189 \dots$). Solid, dashed, dash-dotted, and dotted lines represent the period-doubling, pitchfork, Hopf, and saddle-node bifurcation curves, respectively. Light gray and gray regions denote stability regions of the anti-phase orbits with low periods $P = 4$ and 8 , respectively. (c) Stability diagram obtained by magnifying the rectangular region in (b) with the scaling factors α and δ .

multipliers crosses the unit circle, except at $\lambda = \pm 1$ (*i.e.*, λ becomes a complex number whose magnitude is larger than unity), the orbit loses its stability through a Hopf bifurcation. The type of attractors in the two coupled maps is determined in terms of their Lyapunov exponents (σ_1 and σ_2 ; $\sigma_1 \geq \sigma_2$). By iterating the Jacobian matrix of DT along a trajectory, such Lyapunov exponents are obtained through the Gram-Schmidt reorthonormalization procedure [15]. When the largest Lyapunov exponent σ_1 is negative (zero), the attractor is a periodic (quasiperiodic) one. On the other hand, it is a chaotic one when σ_1 is positive. Furthermore, a hyperchaotic attractor with two positive Lyapunov exponents, σ_1 and σ_2 , may appear.

Figure 1(a) shows four types of periodic orbits in the $x - y$ plane for $a = 1.31$ and $\varepsilon = 0.01$. The symmetric in-phase period-2 orbit with $(P, Q) = (2, 0)$ (represented by solid circles) lies on the diagonal, while the other out-of-phase period-4 orbits with non-zero Q are off the diagonal. The symmetric anti-phase orbit with $(P, Q) = (4, 2)$ is denoted by crosses and a pair of asym-

metric conjugate-phase orbits with $(P, Q) = (4, 1)$ and $(4, 3)$ are represented by up triangles and down triangles, respectively. The stability regions of the symmetric in-phase and anti-phase orbits with low periods are shown in Fig. 1(b). Period-doubling, pitchfork, Hopf, and saddle-node bifurcations occur at the solid, dashed, dash-dotted, and dotted boundary curves, respectively. Particularly, the light-gray and gray regions denote stability regions of the anti-phase orbits with period $P = 4$ and 8, respectively. An anti-phase orbit of type $(4, 2)$ $[(8, 4)]$ appears via a period-doubling bifurcation of the in-phase orbit of type $(2, 0)$ $[(4, 0)]$ at the nonhorizontal solid curve, and it becomes unstable through a Hopf bifurcation at the dash-dotted curve. Using the renormalization method [16–18], it has been shown that near the zero-coupling critical point $(a, \epsilon) = (a^*, 0)$, dynamical behavior at a set of parameters $(a^* + \Delta a, \epsilon)$ is similar to that (with doubled time scale) at a set of scaled parameters $(a^* + \Delta a/\delta, \epsilon/\delta_c)$, where $\Delta a = a - a^*$, and δ ($= 4.669 \dots$) and δ_c are the scaling factors for the nonlinearity and coupling parameters, respectively. For the case of linear coupling of Eq. (1), the scaling is governed by the two relevant factors $\delta_c = \alpha$ ($= -2.502 \dots$) and 2. Hence, the asymptotic scaling associated with coupling is governed by the largest scaling factor α . To see the scaling, we magnify a small rectangular region in Fig. 1(b) with the scaling factors α and δ . The magnified stability diagram with double periods is shown in Fig. 1(c). We note that it is nearly the same as that in Fig. 1(b). Thus, similar anti-phase orbits with higher periods, which lose their stability via Hopf bifurcations, appear successively near the zero-coupling critical point.

Figure 2(a) shows the state diagram near a Hopf bifurcation curve of the anti-phase period-4 orbit. An anti-phase orbit of type $(4, 2)$ appears via a period-doubling bifurcation of the in-phase orbit of type $(2, 0)$ when passing the solid curve $D_{2,0}$. The stability regions of the in-phase orbit and the anti-phase orbit are labeled as their type $(2, 0)$ and $(4, 2)$, respectively. The anti-phase orbit becomes unstable via a Hopf bifurcation at the dash-dotted curve $H_{4,2}$. As a result, mode locking (shown in black) and quasiperiodicity (shown in gray, as in the case of the circle map [1,2]). Some of the mode-locked regions are labeled as their rotation numbers ν , which are just the average numbers of rotations around a mother orbit point per period of the mother orbit (*i.e.*, the anti-phase period-4 orbit). Mode-locked points with the same rotation number ν form a wedge-shaped region (called the “Arnol’d tongue”) fanning out from the Hopf bifurcation point. As the parameter a is further increased, chaos (shown in light gray) and hyperchaos (shown in white) occur. A plot of the rotation number ν versus ϵ along the route, $a = 0.48\epsilon + 1.34$ is given in Fig. 2(b). As ϵ is increased, the rotation number increases. Mode lockings with constant rational rotation number ν (*i.e.*, $\nu = r/s$; r and s : coprimes) occur in parameter intervals; some of them are labeled as their rotation numbers. On the other hand, each quasiperiodicity with an irrational

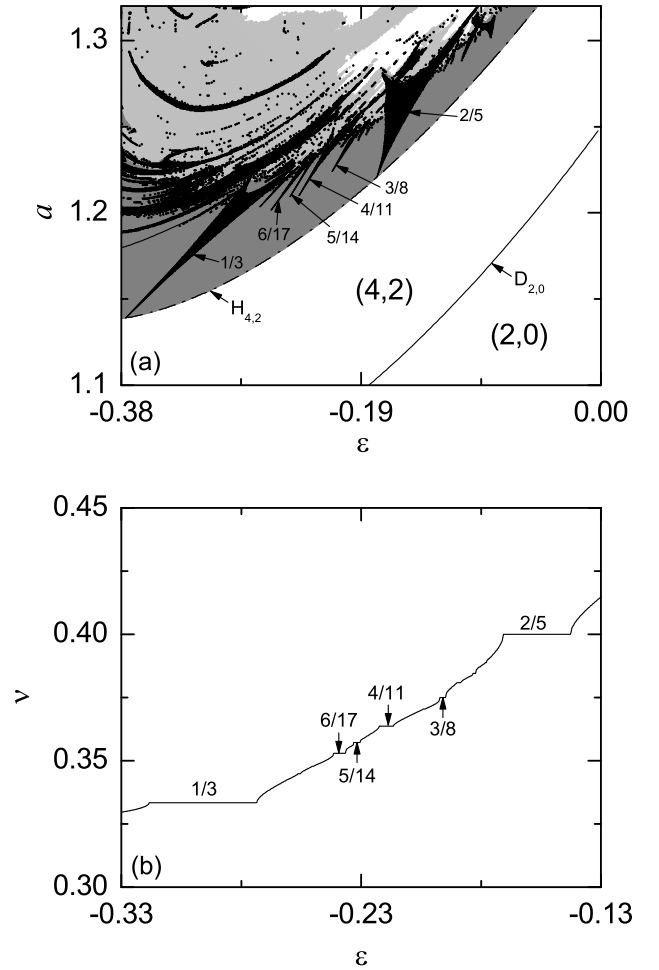


Fig. 2. (a) State diagram near a Hopf bifurcation curve of the anti-phase period-4 orbit. The stability regions of the in-phase and the anti-phase orbits are labeled as their types $(2, 0)$ and $(4, 2)$, respectively. The anti-phase orbit appears via a period-doubling bifurcation when passing the $D_{2,0}$ curve, and it becomes unstable through a Hopf bifurcation at the $H_{4,2}$ curve. Mode locking, quasiperiodicity, chaos, and hyperchaos are shown in black, gray, light gray, and white, respectively. (b) Plot of the rotation number ν versus ϵ along the route, $a = 0.48\epsilon + 1.34$

rotation number ν occurs at a point.

From now on, we investigate the effect of symmetry on Hopf bifurcations of symmetric anti-phase orbits with even periods. A Hopf bifurcation of a symmetric anti-phase orbit occurs when a pair of its stability multipliers $\lambda_{1,2}$ passes the unit circle (where $\lambda_{1,2} = e^{\pm 2\pi i \nu}$) in the complex plane. When ν is an irrational number, a symmetric quasiperiodic attractor with rotation number ν is born, and it encircles the mother anti-phase orbit (denoted by crosses), as shown in Fig. 3(a) for $a = 1.2$ and $\epsilon = -0.25$. However, when ν is a rational number (*i.e.*, $\nu = r/s$; r and s are coprimes), anomalous Hopf bifurcations occur due to the symmetry of the coupled system, which may be analyzed in terms of a half-cycle

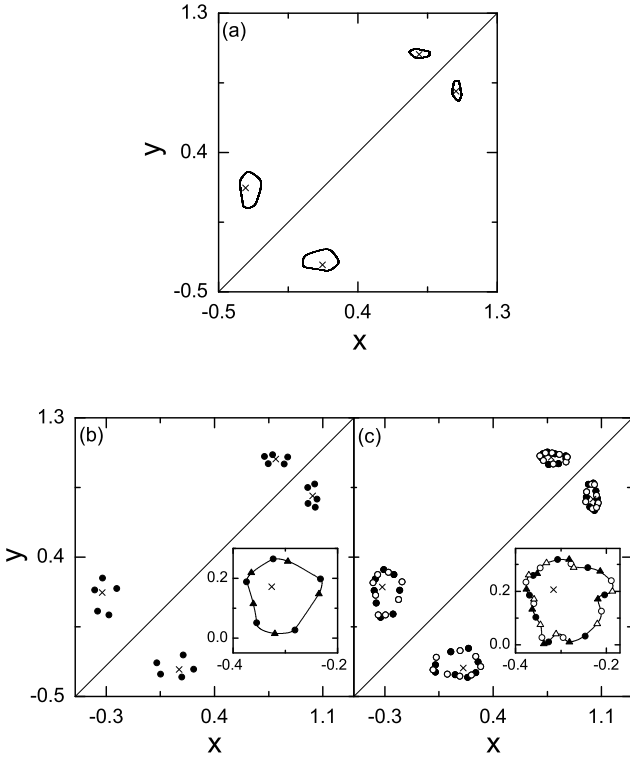


Fig. 3. (a) Symmetric quasiperiodic attractor born via a Hopf bifurcation of the anti-phase period-4 orbit (denoted by crosses) for $a = 1.2$ and $\varepsilon = -0.25$. (b) Symmetry-conserving standard Hopf bifurcation for even r . A pair of symmetric period-20 attractor (denoted by solid circles) and saddle (denoted by solid triangles), born via a standard Hopf bifurcation of the anti-phase period-4 orbit (denoted by crosses), exists for $a = 1.266$ and $\varepsilon = -0.169$ in the Arnol'd tongue with $\nu = 2/5$. The union of the attractor, the saddle, and the unstable manifolds (denoted by solid curves) forms an invariant curve. (c) Symmetry-breaking nonstandard double Hopf bifurcation for odd r . Two conjugate pairs of asymmetric period-32 attractors (denoted by solid and open circles) and saddles (denoted by solid and open triangles), born via a nonstandard Hopf bifurcation of the anti-phase period-4 orbit (denoted by crosses), exist for $a = 1.24$ and $\varepsilon = -0.2$ in the Arnol'd tongue with $\nu = 3/8$. The union of the attractors, the saddles, and the unstable manifolds (denoted by solid curves) forms an invariant curve.

map of the symmetrically-coupled map [13]. We consider a symmetric anti-phase orbit with even period P , $\{\mathbf{z}_n \equiv (x_n, y_n); n = 0, \dots, P - 1\}$. For this case, each orbit point \mathbf{z}_n is a fixed point of the P th iterate of the symmetrically-coupled map T (i.e., T^P), and T^P is the second iterate of a half-cycle map R ,

$$T^P = RR; R = ST^{P/2}. \tag{4}$$

Each point \mathbf{z}_n of the symmetric anti-phase orbit is also a fixed point of R because $S\mathbf{z}_n = \mathbf{z}_{n+P/2}$. We now consider the case that \mathbf{z}_n exhibits a standard Hopf bifurcation in R when its stability multipliers are $e^{\pm 2\pi i p/q}$

(p and q are coprimes). Then, a pair of stable and unstable orbits with rotation number p/q appears in R . For this case, stability multipliers of \mathbf{z}_n in T^P becomes $\lambda[\equiv e^{\pm 2\pi i r/s}] = e^{\pm 2\pi i (2p)/q}$ (r and s are coprimes). For odd q , each daughter orbit in R turns into a daughter orbit with the same period q in T^P which has the rotation number $\nu (= r/s) = 2p/q; r = 2p$ (r : even number). Consequently, for even r , a standard Hopf bifurcation, giving rise to the birth of a pair of stable and unstable orbits with rotation number ν , occurs in T^P . As an example of even r , consider the Arnol'd tongue with rotation number $\nu = 2/5$ in Fig. 2(a). An attractor with $\nu = 2/5$ (denoted by solid circles) encircles its mother anti-phase orbit point (denoted by a cross) in T^4 , as shown in Fig. 3(b) for $a = 1.266$ and $\varepsilon = -0.169$. A magnified view is given in the inset. A pair of attractor (denoted by solid circles) and saddle (denoted by solid triangles) surrounds an anti-phase orbit point. The unstable manifolds (denoted by solid curves) of the saddle points flow into the attractor, and thus form an invariant curve. Thus, a symmetric period-20 daughter attractor, encircling its mother anti-phase period-4 orbit, appears through a standard symmetry-conserving Hopf bifurcation in T . On the other hand, each daughter orbit with even period q (and odd p) in R is transformed into two daughter orbits with periods $q/2$ in T^P , and their rotation numbers in T^P are $\nu (= r/s) = p/(q/2); r = p$ (r : odd number). Consequently, for odd r , two pairs of stable and unstable orbits with rotation number ν appear via a nonstandard double Hopf bifurcation in T^P . As an example of odd r , we consider the Arnol'd tongue with rotation number $\nu = 3/8$ in Fig. 2(a). Two daughter attractors with $\nu = 3/8$ (denoted by solid and open circles) surround their mother anti-phase orbit point (denoted by a cross) in T^4 , as shown in Fig. 3(c) for $a = 1.24$ and $\varepsilon = -0.2$. A magnified view is given in the inset. For this case, the union of two pairs of attractors and saddles (denoted by solid and open triangles) and the unstable manifolds (denoted by solid curves) forms an invariant curve. Thus, a pair of asymmetric period-32 daughter attractors, encircling its mother anti-phase period-4 orbit, appears through a nonstandard symmetry-breaking Hopf bifurcation in T . These two asymmetric attractors are conjugate ones because one attractor is transformed into the other one under an exchange of coordinates S .

To study another type of coupling, called the dissipative coupling, which tends to equalize the states of elements, we consider the following type of two coupled maps:

$$T : \begin{cases} x_{n+1} = f(x_n) + \varepsilon [f(y_n) - f(x_n)], \\ y_{n+1} = f(y_n) + \varepsilon [f(x_n) - f(y_n)]. \end{cases} \tag{5}$$

For this case of dissipative coupling, the scaling, associated with the coupling parameter ε , is governed by only one relevant factor $\delta_c = 2$ [16–18], in contrast to the above case of linear coupling [see Eq. (1)] with $\delta_c = \alpha$ and 2. Figure 4(a) shows stability regions of the symmetric in-phase and anti-phase orbits with low periods.

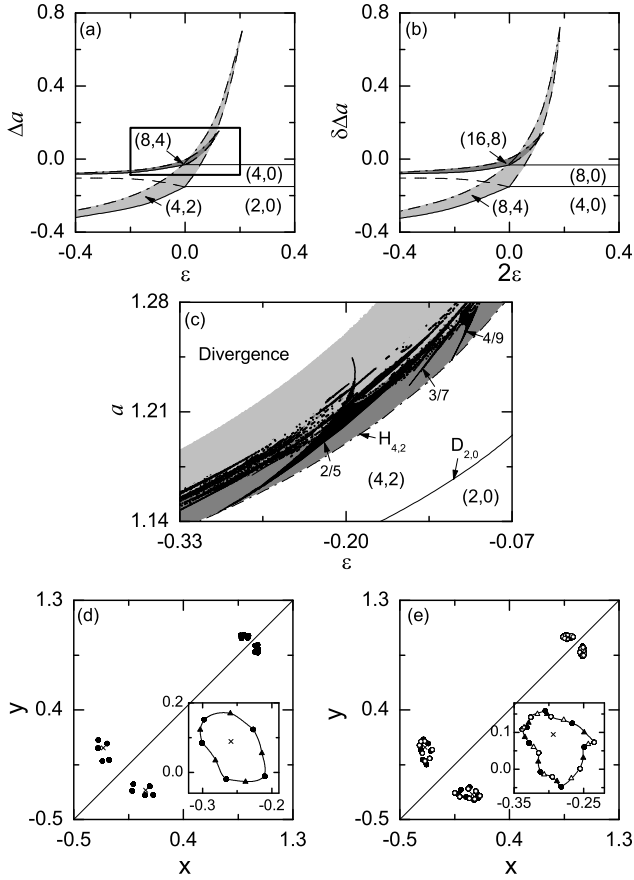


Fig. 4. Hopf bifurcations for the case of dissipative coupling. (a) Stability diagram in the $\varepsilon - \Delta a$ plane. Solid, dashed, and dash-dotted lines denote the period-doubling, pitchfork, and Hopf bifurcation curves, respectively. Light gray and gray regions denote stability regions of the anti-phase orbits with low periods $P = 4$ and 8 , respectively. (b) Stability diagram obtained by magnifying the rectangular region in (a) with the scaling factors 2 and δ . (c) State diagram near a Hopf bifurcation curve of the anti-phase period-4 orbit. The stability regions of the in-phase and the anti-phase orbits are labeled as their types $(2,0)$ and $(4,2)$, respectively. Mode locking, quasiperiodicity, chaos, and divergence are shown in black, gray, light gray, and white, respectively. (d) Symmetry-conserving standard Hopf bifurcation. A symmetric period-20 attractor (denoted by solid circles), born via a standard Hopf bifurcation, exists for $a = 1.208$ and $\varepsilon = -0.2$ in the Arnol'd tongue with $\nu = 2/5$. (e) Symmetry-breaking nonstandard Hopf bifurcation. A conjugate pair of asymmetric period-28 attractors (denoted by solid and open circles), born via a nonstandard double Hopf bifurcations, exists for $a = 1.253$ and $\varepsilon = -0.125$ in the Arnol'd tongue with $\nu = 3/7$.

Period-doubling, pitchfork, and Hopf bifurcations occur at the solid, dashed, and dash-dotted boundary curves, respectively. Stability regions of the anti-phase orbits with period $P = 4$ and 8 are shown in light gray and gray, respectively. These anti-phase orbits appear via period-doubling bifurcations of their in-phase mother orbits

when passing the nonhorizontal solid curves, and they lose their stability via Hopf bifurcations when crossing the dash-dotted curves. To see the scaling, we magnify the small rectangular region in Fig. 4(a) with the scaling factors 2 and δ . The magnified stability diagram with double periods in Fig. 4(b) is nearly the same as that in Fig. 4(a). Thus, similar anti-phase orbits of higher orders, which become unstable via Hopf bifurcations, appear successively near the zero-coupling critical point. Figure 4(c) shows the state diagram near the dash-dotted Hopf bifurcation curve $H_{4,2}$ of the anti-phase orbit with $(P, Q) = (4, 2)$, which is born via a period-doubling bifurcation of the in-phase orbit of type $(2, 0)$ when passing the solid curve $D_{2,0}$. As in the linear-coupling case, mode-locking (shown in black) and quasiperiodicity (shown in gray) occur via Hopf bifurcations of the anti-phase period-4 orbit. Some Arnol'd tongues are labeled with their rotation numbers. With further increase in a , chaos and divergence occur in the light-gray and the white regions, respectively. As shown in the above, for the case of rational rotation number $\nu (= r/s)$, a standard or a nonstandard Hopf bifurcation may occur, depending on whether r is even or odd. As an example of even r , we consider the Arnol'd tongue with $\nu = 2/5$. A daughter attractor with the rotation number $\nu = 2/5$ (denoted by solid circles) encircles its mother anti-phase orbit point (denoted by a cross) in T^4 , as shown in Fig. 4(d) for $a = 1.208$ and $\varepsilon = -0.2$. A magnified view is given in the inset. The union of the attractor, the saddle (denoted by solid triangles), and the unstable manifold forms an invariant curve. Thus, a symmetric period-20 attractor, encircling its mother anti-phase period-4 orbit, appears via a standard symmetry-conserving Hopf bifurcation in T . As an example of odd r , we consider the Arnol'd tongue with $\nu = 3/7$. As shown in Fig. 4(e) for $a = 1.253$ and $\varepsilon = -0.125$, two attractors (denoted by solid and open circles with $\nu = 2/5$ in T^4) surround their mother anti-phase orbit point (denoted by a cross). The union of two pairs of attractors and saddles (denoted by solid and open triangles) and unstable manifolds forms an invariant curve (see the magnified view in the inset). Thus, a conjugate pair of asymmetric period-28 attractors, encircling its mother anti-phase period-4 orbit, appears via a nonstandard symmetry-breaking Hopf bifurcation in T .

III. SUMMARY

For both cases of linear and dissipative couplings, we have investigated the effect of symmetry on Hopf bifurcations of symmetric anti-phase periodic orbits in two symmetrically-coupled logistic maps. When the rotation numbers ν of daughter orbits are rational (*i.e.*, $\nu = r/s$), two types of Hopf bifurcations occur due to the symmetry of the coupled system. For even r , a symmetric periodic attractor appears through a standard Hopf bifurcation while for odd r , a conjugate pair of asym-

metric attractors is born via a nonstandard double Hopf bifurcation. These anomalous Hopf bifurcations are explained by using the concept of a half-cycle map of a symmetrically-coupled map. In the presence of small asymmetry, Hopf bifurcations also occur [11]. However, they are only standard ones, unlike the symmetric case. Finally, the symmetry-conserving and -breaking Hopf bifurcations should be observed in real experiments of symmetrically-coupled period-doubling systems such as two resistively-coupled p-n junction resonators [9] and two inductively-coupled electronic frequency generators [10].

REFERENCES

- [1] S. J. Shenker, *Physica D* **5**, 405 (1982); M. J. Feigenbaum, L. P. Kadanoff and S. J. Shenker, *Physica D* **5**, 370 (1982); D. Rand, O. Ostlund, J. Sethna and E. Siggia, *Phys. Rev. Lett.* **49**, 132 (1982).
- [2] M. H. Jensen, P. Bak and T. Bohr, *Phys. Rev. A* **30**, 1960 (1984).
- [3] K. Kaneko, *Prog. Theor. Phys.* **69**, 1427 (1983).
- [4] J.-M. Yuan, M. Tung, D. H. Feng and L. M. Narducci, *Phys. Rev. A* **28**, 1662 (1983).
- [5] J. Frøyland, *Physica D* **8**, 423 (1983).
- [6] T. Hogg and B. A. Huberman, *Phys. Rev. A* **29**, 275 (1984).
- [7] X. Wang and R. Mainieri, *Phys. Rev. A* **40**, 5382 (1989).
- [8] J. Rasmussen, E. Mosekilde and C. Reick, *Math. Comput. Simul.* **40**, 247 (1996).
- [9] R. Van Buskirk and C. Jeffries, *Phys. Rev. A* **31**, 3332 (1985).
- [10] V. S. Anishchenko, *Dynamical Chaos in Physical Systems* (Teubner, Leipzig, 1989).
- [11] C. Reick and E. Mosekilde, *Phys. Rev. E* **52**, 1418 (1995).
- [12] E. N. Erastova and S. P. Kuznetsov, *Sov. Phys. Tech. Phys-U.* **36**, 130 (1991).
- [13] J. W. Swift and K. Wiesenfeld, *Phys. Rev. Lett.* **52**, 705 (1984).
- [14] M. J. Feigenbaum, *J. Stat. Phys.* **19**, 25 (1978); *ibid* **21**, 669 (1979).
- [15] A. J. Lichtenberg and M. A. Leiberman, *Regular and Stochastic Motion* (Springer-Verlag, New York, 1983), p. 283.
- [16] S. Kuznetsov, *Radiophys. Quantum El.* **28**, 681 (1985).
- [17] H. Kook, F. H. Ling and G. Schmidt, *Phys. Rev. A* **43**, 2700 (1991).
- [18] S.-Y. Kim and H. Kook, *Phys. Rev. E* **48**, 785 (1993); *ibid* *Phys. Rev. A* **46**, R4467 (1992); *ibid* *Phys. Lett. A* **178**, 258 (1993).